Plasma Phys. Control. Fusion **42** (2000) 545–555. Printed in the UK PII: S0741-3335(00)11893-7

Effects of non-circular tokamak geometry on ion-temperature-gradient driven modes

J Anderson, H Nordman and J Weiland

Department of Electromagnetics, EURATOM-NFR Association, Chalmers University of Technology, Göteborg, Sweden

Received 16 February 2000

Abstract. The influence of plasma elongation and Shafranov shift on the stability of electrostatic ion-temperature-gradient driven modes (η_i-modes) is investigated. An advanced fluid model is used for the ions together with Boltzmann distributed electrons. The derived eigenvalue equation is solved both analytically, in the strong ballooning limit, and numerically. It is found that the effects of elongation change from stabilizing, for peaked density profiles, to destabilizing in the flat density regime. In addition, it is shown that the maximum growth rate is shifted towards shorter wavelengths as the elongation increases. The effects of shaping on tokamak stability are exemplified with data from a Joint European Torus (JET) high-performance mode discharge.

1. Introduction

One of the main challenges of fusion research is to understand the anomalously high transport of particles and energy in magnetically confined plasmas [1, 2]. Although substantial progress has recently been made in this field, some unsolved problems remain.

One of the most important is that of the effects of plasma shaping. The beneficial effects of elongation on MHD stability are well established and understood. The effects on transport are, however, not yet well understood. Empirically, it is known that elongation has a favourable influence on transport [3]. While the explicit dependence of the confinement time on elongation is roughly as $\kappa^{0.5}$, another important effect is through the current scaling since the plasma cross section, and thereby the current, increases with elongation.

One of the effects of elongation is to modify the perpendicular space variation and thereby the effective magnetic shear [4]. This has a beneficial effect on MHD stability since the stabilizing Alfvén frequency enters together with the squared perpendicular mode number. On drift waves we get an enhanced convective damping due to magnetic shear. At the same time, however, the mode width is reduced and this tends to reduce the beneficial effect on shear damping. The net effect can even sometimes be destabilizing [5].

As found in the present work, the effect of elongation on the magnetic drift can also be important. This is, in particular, the case for modes localized at the outside of the torus since the poloidal curvature there is reduced by elongation. The ion-temperature-gradient driven mode is one of the main candidates for explaining the anomalous transport in tokamaks [6–9]. A few studies of η_i-mode [4, 10, 11] and trapped electron mode [12, 13] stability in the presence of flux surface shaping have been made before. Two linear papers [4, 10] show weak stabilizing effects of elongation while recent nonlinear work is less decisive [11]. As compared to the linear studies, we have made here an extension to include the effects of elongation on the

0741-3335/00/050545+11$30.00

magnetic drift frequency. We also note that the sensitivity of drift waves to effects of geometry depends strongly on the fluid closure. It is thus essential to study effects of elongation with an advanced fluid model, such as the one used here. This model has been successful in reproducing both experimental [14] and nonlinear gyro-kinetic results [15].

The paper is organized as follows. In section 2 the model equations and the equilibrium are discussed. In section 3, the effects of elongation and Shafranov shift on the stability of ion-temperature-gradient modes are discussed. Finally, a brief summary is given in section 4.

2. Formulation

An advanced fluid model [16–19] is used for the ion physics whereas the electrons are assumed to be Boltzmann distributed. The model equations are solved utilizing a generalized non-circular equilibrium model [20] which allows for controlled variation of the shape parameters like elongation and Shafranov shift. Focusing on the fluid model, we start with the ion continuity, the ion energy and the parallel momentum equation. In the electrostatic limit, the equations take the forms

$$\frac{\partial n_\mathrm{i}}{\partial t} + \nabla \cdot (n_\mathrm{i}\vec{v}_E + n_\mathrm{i}\vec{v}_{\star\mathrm{i}}) + \nabla \cdot (n_\mathrm{i}\vec{v}_{p_\mathrm{i}} + n_\mathrm{i}\vec{v}_{\pi\mathrm{i}}) + \nabla \cdot (n_\mathrm{i}\vec{v}_{\|\mathrm{i}}) = 0 \tag{1}$$

$$m_\mathrm{i} n_\mathrm{i} \frac{\partial \vec{v}_{\|\mathrm{i}}}{\partial t} + \nabla_\| p_\mathrm{i} + n_\mathrm{i} e \nabla_\| \phi = 0 \tag{2}$$

$$\frac{3}{2} n_\mathrm{i} \frac{\mathrm{d}T_\mathrm{i}}{\mathrm{d}t} + n_\mathrm{i} T_\mathrm{i} \nabla \cdot \vec{v}_\mathrm{i} + \nabla \cdot \vec{q}_\mathrm{i} = 0. \tag{3}$$

Here, n_i is the ion particle density, $p_\mathrm{i} = n_\mathrm{i} T_\mathrm{i}$ is the ion pressure, T_i is the ion temperature, $\vec{v}_{\|\mathrm{i}}$ is the parallel ion velocity, ϕ is the electrostatic potential, and m_i is the ion mass. The convective derivative is defined as $\mathrm{d}/\mathrm{d}t = \partial/\partial t + (\vec{v}_E + \vec{v}_{\star\mathrm{i}}) \cdot \nabla$. The diamagnetic and $\vec{E} \times \vec{B}$ drifts are defined as

$$\vec{v}_{\star\mathrm{i}} = \frac{c}{e n_\mathrm{i} B}(e_\| \times \nabla p_\mathrm{i}) \tag{4}$$

$$\vec{v}_E = \frac{c}{B}(e_\| \times \nabla \phi) \tag{5}$$

where e is the charge, c is the speed of light, and $e_\| = \vec{B}/|\vec{B}|$ is a unit vector along the magnetic field. The drift $\vec{v}_{\pi\mathrm{i}}$ is the stress tensor drift and the polarization drift v_{p_i} is defined as

$$\vec{v}_{p_\mathrm{i}} = \frac{1}{\Omega_\mathrm{ci}} \left(\frac{\partial}{\partial t} + \vec{v}_\mathrm{i} \cdot \nabla \right) (e_\| \times \vec{v}_\mathrm{i}) \tag{6}$$

where $\vec{v}_\mathrm{i}$ is the total ion drift velocity and the cyclotron frequency is given by $\Omega_\mathrm{ci} = eB/m_\mathrm{i}c$. Here we express the divergence as

$$\nabla \cdot (n_\mathrm{i}\vec{v}_{p_\mathrm{i}} + n_\mathrm{i}\vec{v}_{\pi\mathrm{i}}) = \nabla \cdot \left(\frac{n_\mathrm{i}}{\Omega_\mathrm{ci}} \frac{\partial}{\partial t} (e_\| \times \vec{v}_\mathrm{i}) \right)$$

where we substitute $\vec{v}_E$ and $\vec{v}_{\star\mathrm{i}}$ for $\vec{v}_\mathrm{i}$. The part due to $\vec{v}_E$ corresponds to the polarization drift velocity and the part due to $\vec{v}_{\star\mathrm{i}}$ is the lowest-order finite Larmor radius (FLR) term. We then obtain

$$\nabla \cdot (n_\mathrm{i}\vec{v}_{p_\mathrm{i}} + n_\mathrm{i}\vec{v}_{\pi\mathrm{i}}) = -n_\mathrm{i}\rho_\mathrm{s}^2 \frac{\partial}{\partial t} \Delta \frac{e\phi}{T_\mathrm{e}} - \frac{\rho_\mathrm{s}^2}{T_\mathrm{e}} \frac{\partial}{\partial t} \Delta \delta p_\mathrm{i} \tag{7}$$

where $\rho_\mathrm{s} = c_\mathrm{s}/\Omega_\mathrm{ci}$ and $c_\mathrm{s} = \sqrt{T_\mathrm{e}/m_\mathrm{i}}$. The diamagnetic ion heat flux is given by

$$\vec{q}_\mathrm{i} = \vec{q}_{\star\mathrm{i}} = \frac{5}{2} \frac{c T_\mathrm{i} n_\mathrm{i}}{eB} e_\| \times \nabla T_\mathrm{i}. \tag{8}$$

The ion temperature fluctuations equations couple to equations (1) and (2) through

$$\nabla \cdot (n_j \vec{v}_{\star j}) = \frac{1}{T_j} \vec{v}_{Dj} \cdot \nabla \delta P_j \tag{9}$$

where δP_j ($j = \mathrm{i}, \mathrm{e}$) is the perturbed pressure and $\vec{v}_{\mathrm{D}j}$ is the magnetic drift velocity at the thermal speed, i.e.

$$\vec{v}_{\mathrm{Di}} = \frac{T_\mathrm{i}}{m_\mathrm{i}\Omega_\mathrm{ci}} \left[\frac{e_\parallel \times \nabla B}{B} + e_\parallel \times \vec{\kappa} \right] \tag{10}$$

where $\vec{\kappa} = (e_\parallel \cdot \nabla) e_\parallel$ is the curvature vector. Additional curvature relations arise in equations (1) and (2) as

$$\nabla \cdot \vec{q}_{\star \mathrm{i}} = -\frac{5}{2} n_\mathrm{i} \vec{v}_{\star \mathrm{i}} \cdot \nabla T + \frac{5}{2} n_\mathrm{i} \vec{v}_{\mathrm{Di}} \cdot \nabla T \tag{11}$$

$$\nabla \cdot \vec{v}_E = \frac{q_j}{T_j} \vec{v}_{\mathrm{D}j} \cdot \nabla \phi. \tag{12}$$

Assuming a perturbation of the form $\mathrm{e}^{-\mathrm{i}\omega t}$ and using the continuity equation for $\nabla \cdot \vec{v}_\mathrm{i}$ in the energy equation, the convective diamagnetic effects cancel out and the energy equation becomes

$$\frac{\delta T_\mathrm{i}}{T_\mathrm{i}} = \frac{\omega}{\omega - \frac{5}{3}\omega_{\mathrm{Di}}} \left(\frac{2}{3} \frac{\delta n_\mathrm{i}}{n_0} - \frac{\omega_{\star \mathrm{e}}}{\omega} \left(\frac{2}{3} - \eta_\mathrm{i} \right) \frac{e\phi}{T_\mathrm{e}} \right). \tag{13}$$

The parallel ion equation (2) gives

$$\vec{v}_{\parallel \mathrm{i}} = -\mathrm{i} \frac{c_\mathrm{s}^2}{\omega} e_\parallel \cdot \nabla \left(\frac{e\phi}{T_\mathrm{e}} + \frac{1}{\tau} \frac{\delta p_\mathrm{i}}{p_\mathrm{i}} \right). \tag{14}$$

Here we have $\tau = T_\mathrm{e}/T_\mathrm{i}$ and $\eta_\mathrm{i} = \mathrm{d} \ln T_\mathrm{i} / \mathrm{d} \ln n_\mathrm{i}$. Substituting (13) and (14) into (1) and using quasineutrality and Boltzmann distributed electrons $\delta n_\mathrm{i}/n_0 = \delta n_\mathrm{e}/n_0 = e\phi/T_\mathrm{e}$ we arrive at the eigenvalue equation

$$c_\mathrm{s}^2 (e_\parallel \cdot \nabla)^2 \left(1 + \frac{1}{\tau} + \hat{F} \right) \frac{e\phi}{T_\mathrm{e}} = -\omega(\omega - \omega_{\star \mathrm{e}}) \frac{e\phi}{T_\mathrm{e}} + \omega(\tau \omega_{\mathrm{Di}} - \omega k_\perp^2 \rho_\mathrm{s}^2) \left(1 + \frac{1}{\tau} + \hat{F} \right) \frac{e\phi}{T_\mathrm{e}} \tag{15}$$

where

$$\hat{F} = \frac{\omega}{\omega - \frac{5}{3}\omega_{\mathrm{Di}}} \left(\frac{2}{3\tau} + \frac{\omega_{\star \mathrm{i}}}{\omega} \left(\frac{2}{3} - \eta_\mathrm{i} \right) \right). \tag{16}$$

Employing the standard high-n ballooning mode formalism [21], we obtain a second-order eigenvalue equation for the potential ϕ in the extended poloidal angle θ,

$$\frac{\partial^2 \psi}{\partial \theta^2} = -h \left(\left(1 - \frac{1}{\Omega} \right) A + \frac{\epsilon_n}{\Omega} g(\theta) + b \right) \psi \tag{17}$$

where $\Omega = \omega/\omega_\star$ and we have

$$\psi = \left(1 + \frac{1}{\tau} + \hat{F} \right) \frac{e\phi}{T_\mathrm{e}} \tag{18}$$

$$A = \frac{1 + (5/3\tau)/(\epsilon_n/\Omega) g(\theta)}{F + \beta(\epsilon_n/\Omega) g(\theta)} \tag{19}$$

$$F = 1 + \frac{1}{\Omega\tau}(1 + \eta_\mathrm{i}) + \frac{5}{3\tau} \left(1 - \frac{1}{\Omega} \right) \tag{20}$$

$$\beta = \frac{5}{3\tau} \left(1 + \frac{1}{\tau} \right) \tag{21}$$

$$h = \frac{g_{\theta\theta} q^2 k_\theta^2 \rho_{\mathrm{i}}^2 \tau \Omega^2}{2\epsilon_n^2} \tag{22}$$

$$\omega_{\mathrm{D}} = \omega_\star \epsilon_n g(\theta) \tag{23}$$

$$k_\perp^2 = k_\theta^2 k(\theta). \tag{24}$$

Here, $\epsilon_n = \omega_{\mathrm{D}}/\omega_\star = 2L_n/L_B$ and q is the safety factor, $s = \mathrm{d}\ln q/\mathrm{d}\ln r$ is the magnetic shear. The geometric effects enters through the magnetic drift frequency ω_{D} and the scale factor $\sqrt{g_{\theta\theta}}$ in the second-order differential eigenvalue equation and through $k_\perp^2$. The equilibrium model used is a generalization of the $s-\alpha$ equilibrium model developed in [20]. The flux surface coordinate system is defined by

$$R(r,\theta) = \sum_{n=0}^{\infty} R_n(r)\cos(n\theta) \tag{25}$$

$$Z(r,\theta) = \sum_{n=0}^{\infty} Z_n(r)\sin(n\theta) \tag{26}$$

where R and Z are the usual cylindrical coordinates. The terms R_0, $R_1 = r$, $Z_1 = r\kappa$ describe shift, minor radius and ellipticity, respectively, the terms R_2, Z_2 describe triangularity. In the present work effects of triangularity are neglected. The scale factors become

$$g_{rr} = (\partial_r R_0 + \cos\theta)^2 + (\partial_r(r\kappa)\sin\theta)^2 \tag{27}$$

$$g_{\theta\theta} = r^2(1 + (\kappa^2 - 1)\cos^2\theta) \tag{28}$$

$$g_{r\theta} = (\partial_r(\kappa r)\kappa r \sin\theta\cos\theta - r(\partial_r R_0 + \cos\theta)\sin\theta) \tag{29}$$

$$g_{\phi\phi} = R^2 \tag{30}$$

where κ is the elongation and $\partial_j = \partial/\partial x^j$; note that it only acts at the object directly after and we denote position vector $\vec{r} = (R, Z)$ and basis vectors $\hat{e}_j = (1/h_j)\partial_j \vec{r}$. The metric tensor g_{ij} is defined as

$$\mathrm{d}s^2 = g_{ij}\,\mathrm{d}x^i\,\mathrm{d}x^j. \tag{31}$$

Keeping only the first terms in ϵ-ordering and under the assumption that the B-field is $\vec{B} = B_\theta\hat{\theta} + B_\phi\hat{\phi}$, we have the magnetic drift frequency and $k_\perp$ as

$$\frac{\omega_{\mathrm{D}}}{\omega_{\star\mathrm{e}}} = \epsilon_n g(\theta) \approx \frac{\epsilon_n}{\sqrt{g_{\phi\phi}}}\left(g^{\theta r}\Gamma^r_{\phi\phi} J\frac{q}{r}s + g^{\theta\theta}\Gamma^r_{\phi\phi} Jq - g^{rr}\Gamma^\theta_{\phi\phi} J\frac{q}{r}s - g^{\theta r}\Gamma^\theta_{\phi\phi} Jq\right) \tag{32}$$

$$k_\perp^2 = k_\theta^2 k(\theta) \approx -\frac{k_\theta^2}{J^2}(g_{rr} + g_{\theta\theta}(s\theta)^2 + 2g_{r\theta}s\theta). \tag{33}$$

Here the inverse of the metric tensor is defined by the relation $g_{ij}g^{jk} = \delta_{\mathrm{i}}^k$, compare with (33). The Christoffel symbols are given by

$$\Gamma^i_{jk} = \frac{1}{2}g^{jn}(\partial_k g_{ni} + \partial_i g_{nk} - \partial_j g_{ik}) \tag{34}$$

$$\Gamma^r_{\phi\phi} = -\frac{1}{4}\left(\frac{g_{rr}}{J^2}\partial_r g^2_{\phi\phi} + \frac{g_{r\theta}}{J^2}\partial_\theta g^2_{\phi\phi}\right) \tag{35}$$

$$\Gamma^\theta_{\phi\phi} = -\frac{1}{4}\left(\frac{g_{\theta r}}{J^2}\partial_r g^2_{\phi\phi} + \frac{g_{\theta\theta}}{J^2}\partial_\theta g^2_{\phi\phi}\right) \tag{36}$$

where the Jacobian is given by

$$J^2 = g_{\phi\phi}(g_{rr}g_{\theta\theta} - g^2_{r\theta}). \tag{37}$$

These results reduce to the usual expressions in circular geometry, i.e.

$$\frac{\omega_{\mathrm{D}}}{\omega_{\star \mathrm{e}}} \approx \epsilon_n(\cos\theta + s\theta\sin\theta) \tag{38}$$

$$k_\perp^2 \approx k_\theta^2(1 + s^2\theta^2). \tag{39}$$

The eigenfunctions are often well localized corresponding to the strong ballooning limit. Expanding all expressions for small theta to second order we get the Weber equation

$$\frac{\partial^2\psi}{\partial\theta^2} = (A(\Omega) - B(\Omega)\theta^2)\psi. \tag{40}$$

The solution is given in the Hermite polynoms as

$$\psi_n(\theta) = H_n(B^{\frac{1}{4}}\theta)\,\mathrm{e}^{-\frac{1}{2}B^{\frac{1}{2}}\theta^2} \tag{41}$$

where we require that $\mathrm{Re}[B^{\frac{1}{2}}] > 1$ for strong localization. The analytically obtained η_{i}-mode growth rate will be compared with the numerical solutions later. However, this approximation method has some limitations. For example to ensure that we get a well localized mode we have to consider rather small ϵ_n to get good agreement with the numerical result.

3. Effects of non-circular geometry: results and discussion

The eigenvalue equation (17) is solved numerically using a standard shooting technique. We focus on the even modes since they are expected to be more important for tokamak confinement than the odd modes. Starting from $\theta = 0$ with $\psi(0) = 1$ and $\psi'(0) = 0$, the eigenvalue is iterated until the condition $\psi \to 0$ as $\theta \to \infty$ is satisfied.

In figure 1 the effects of elongation κ on the η_{i}-mode stability are illustrated. The growth rate (normalized to the electron diamagnetic frequency) as a function of η_{i} is shown with ϵ_n $(2L_n/L_B)$ and κ as a parameter. The other parameters are $q = s = \tau = 1$ and $k_\perp^2\rho^2 = 0.1$. The results are shown for $\epsilon_n = 1$, $\kappa = 1.5$ (curve a1) and $\kappa = 1$ (curve a2), and for $\epsilon_n = 0.1$, $\kappa = 1.5$ (curve b1) and $\kappa = 1$ (curve b2). A slight destabilization of the mode with increasing κ is found for both peaked ($\epsilon_n = 0.1$) and flat ($\epsilon_n = 1$) density profiles in this parameter

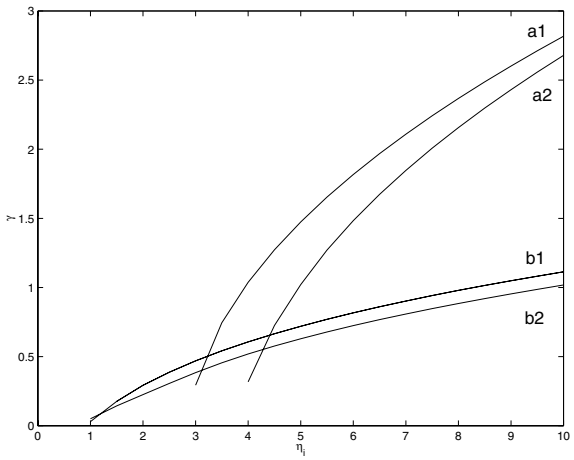

Figure 1. The growth rate (normalized to the electron diamagnetic drift frequency) versus η_{i}, for $q = s = \tau = 1$, $k_\perp^2\rho^2 = 0.1$, $\epsilon_n = 1$, $\kappa = 1.5$ (curve a1); $\epsilon_n = 1$, $\kappa = 1$ (curve a2); $\epsilon_n = 0.1$, $\kappa = 1.5$ (curve b1) and $\epsilon_n = 0.1$, $\kappa = 1$ (curve b2).

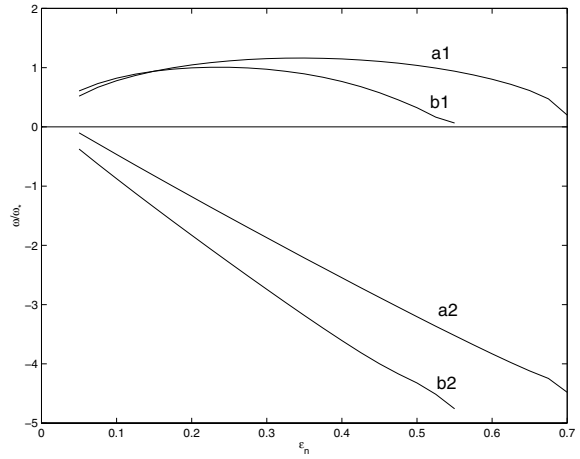

Figure 2. The growth rate (normalized to the electron diamagnetic drift frequency) versus ϵ_n, for $q = s = \tau = 1$, $k_\perp^2\rho^2 = 0.1$, $\eta_\mathrm{i} = 4$, $\kappa = 1.5$ (curves a1 and a2); $\kappa = 1$ (curves b1 and b2).

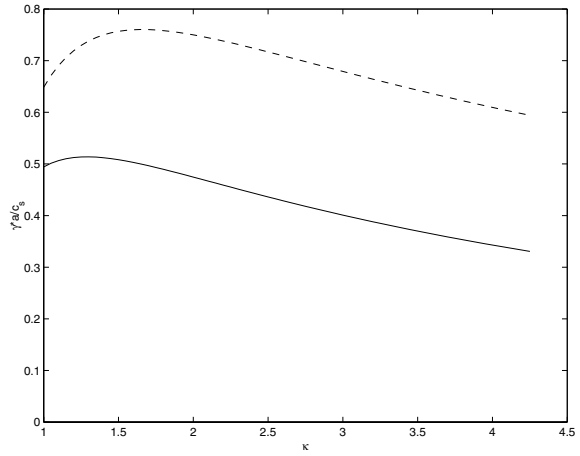

Figure 3. The growth rate (normalized to c_s/a) versus κ for $q = 2$, $s = \tau = 1$, $k_\perp^2\rho^2 = 0.16$, $\eta_\mathrm{i} = 6$, $\epsilon_n = 0.33$ (full curve) and $\epsilon_n = 1.0$ (dashed curve).

regime. Close to marginal stability, the destabilizing effects of elongation are substantial, in particular for flat density profiles.

In figure 2 the ϵ_n dependence of the eigenvalue (both real frequency and growth rate) with κ is displayed. The other parameters are as in figure 1 with $\kappa = 1$ (curves b1, b2) and $\kappa = 1.5$ (curves a1, a2). The mode is stabilized for large ϵ_n due to compressional effects. We note that the effects of elongation are destabilizing in the flat density limit whereas for peaked density profiles, $\epsilon_n \leqslant 0.15$, the effects are stabilizing. Elongation also results in an increase of $|\omega_r|$.

Earlier work indicates that the η_i-mode growth rate is reduced with increasing elongation [4, 10, 11]. To illustrate this, figure 3 shows the effects of elongation on the growth rate with parameters taken from [11] with $q = 2$, $s = \tau = 1$, $k_\perp^2\rho^2 = 0.16$, $\eta_\mathrm{i} = 6$ and $\epsilon_n = 0.33$ (full curve, cf figure 2(b) of [11]) and $\epsilon_n = 1$. For peaked density profiles $\epsilon_n = 0.33$ (full curve) the effects of elongation are found to be stabilizing in good qualitative agreement with the

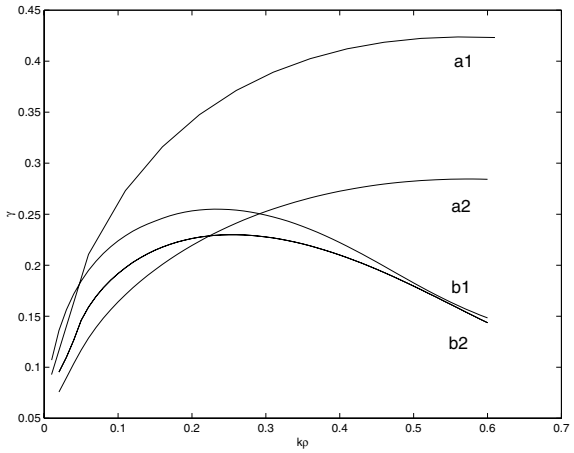

Figure 4. The growth rate versus $k_\perp \rho$ for $q = s = \tau = 1$, $\eta_\mathrm{i} = 4$, $\epsilon_n = 0.1$. The curves a1 ($\kappa = 1.5$) and b1 ($\kappa = 1$) are the analytical dispersion relations and a2 ($\kappa = 1.5$) and b2 ($\kappa = 1$) are the numerical simulations.

results reported in [11]. For flat density profiles $\epsilon_n = 1$ (dashed curve), on the other hand, a substantial destabilization is found for $\kappa \leqslant 1.7$. As the equilibria becomes more elongated the influence of κ is reversed and a stabilization is observed for large values of κ.

Next, the effects of κ on the k_θ spectrum are discussed. Figure 4 displays the mode growth as a function of $k_\theta \rho$ with κ as a parameter. The parameters are as in figure 1 except that we have fixed $\epsilon_n = 0.1$ and have $\kappa = 1.5$ for the curve a2 and $\kappa = 1$ for the curve b2. In the circular case ($\kappa = 1$) the maximum growth rate occurs for $k_\theta \rho_\mathrm{s} = 0.3$. For $\kappa = 1.5$, however, the peak is shifted towards larger values of $k_\theta \rho$. Also shown is the analytical solution, for $\kappa = 1.5$ (curve a1) and $\kappa = 1$ (curve b1) in the strong ballooning limit (equation (40)). The analytical approximation usually overestimates the growth rate for elongated equilibria, whereas the circular case is well reproduced.

Figure 5 illustrates the effects of elongation in combination with negative shear on η_i-mode stability. The normalized growth rate is shown as function of η_i with κ and s as parameters. The other parameters are $q = 2$, $\epsilon_n = 0.2$, $\tau = 1$ and for $s = 0.5$ we have $\kappa = 1.5$ (curve a1) and $\kappa = 1.0$ (curve a2), whereas for $s = -0.5$ we have $\kappa = 1$ (curve b2) and $\kappa = 1.5$ (curve b1). For the circular case, the effects of negative shear ($s = -0.5$ versus $s = 0.5$) are slightly stabilizing. For $\kappa = 1.5$, on the other hand, a substantial reduction in growth rate is obtained in the negative shear case. The results indicate that the stabilizing effects of magnetic shear can be enhanced in the presence of elongated equilibria.

In figure 6 the modulus of the eigenfunction is shown for $\epsilon_n = 1$ (full curve) and $\epsilon_n = 0.1$ (dashed curve). The other parameters are as in figure 1 with $\kappa = 1$. The eigenmode tends to be more localized for small ϵ_n. In this regime, however, the eigenmode is rather insensitive to elongation. We thus expect the strong ballooning approximation (equation (40)) to be valid for small ϵ_n.

In the eigenvalue equation (equation (17)), the effects of elongation enter through the magnetic drift frequency $\omega_\mathrm{D} = \omega_\star \epsilon_n g(\theta)$, the FLR parameter $k_\perp^2 = k_\theta^2 k(\theta)$ and the mode structure along the field line ($k_\parallel$). Since the effects on the mode structure are usually small the main effects enter through ω_D and $k_\perp^2$. In figures 7(a) and 7(b), the influence of κ on $\omega_\mathrm{D}(\theta)$ and $k_\perp^2(\theta)$ are illustrated. In figures 7(a) and 7(b) $\omega_\mathrm{D}(\theta)$ and $k(\theta)$ are given for $\kappa = 1$ (full curve) and for $\kappa = 1.5$ (dashed curve). We note that $g(\theta = 0)$ is reduced with increasing elongation

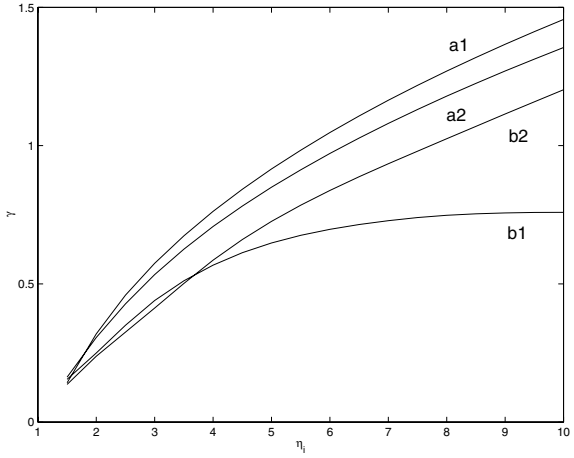

Figure 5. The growth rate (normalized to the electron diamagnetic drift frequency) versus η_i for $q = 2$, $\tau = 1$, $k_\perp^2\rho^2 = 0.1$, $\epsilon_n = 0.2$. The curves a1 ($\kappa = 1.5$) and a2 ($\kappa = 1$) have $s = 0.5$; the curves b1 ($\kappa = 1$) and b2 ($\kappa = 1.5$) have $s = -0.5$.

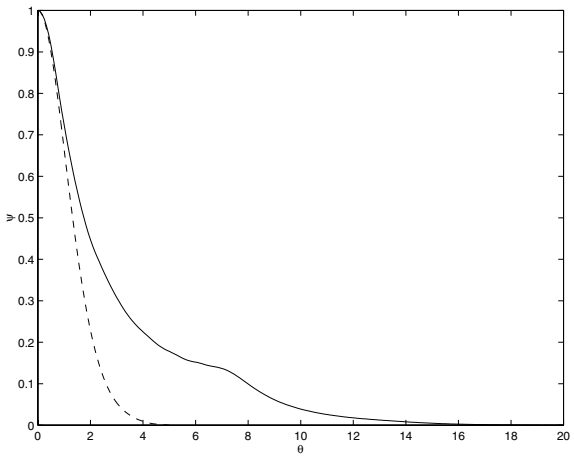

Figure 6. The eigenfunctions for different ϵ_n with $q = s = \tau = 1$, $k_\perp^2\rho^2 = 0.1$, $\eta_i = 4$ where $\epsilon_n = 1$ (full curve) and $\epsilon_n = 0.1$ (dashed curve).

(figure 7(a), dashed curve). Also $k_\perp^2(\theta = 0)$ is slightly reduced in the $\kappa = 1.5$ (dashed curve) case.

In order to quantify and compare the effects of elongation (through ω_D and $k_\perp^2$) on the mode growth we solve (equation (17)) while artificially keeping the magnetic drift ω_D at its circular value. The results of a κ-scaling with ϵ_n as a parameter are shown in figure 8. The growth rates (curve a2, $\epsilon_n = 1$; curve b1, $\epsilon_n = 0.1$) are then compared with the solution to (equation (17)) with the full κ-dependence retained (curve a1, $\epsilon_n = 1$; curve b2, $\epsilon_n = 0.1$). As observed, the inclusion of the κ-dependence of the magnetic drift can be both stabilizing ($\epsilon_n = 0.1$) and destabilizing ($\epsilon_n = 1$). This is a consequence of the ϵ_n-dependence of the mode growth as displayed in figure 2. As κ increases, $\omega_D(0)$ is reduced (figure 6(a)) and this leads to an effective reduction of $\epsilon_n = \omega_D(0)/\omega_\star$. The resulting effect on the growth is stabilizing close

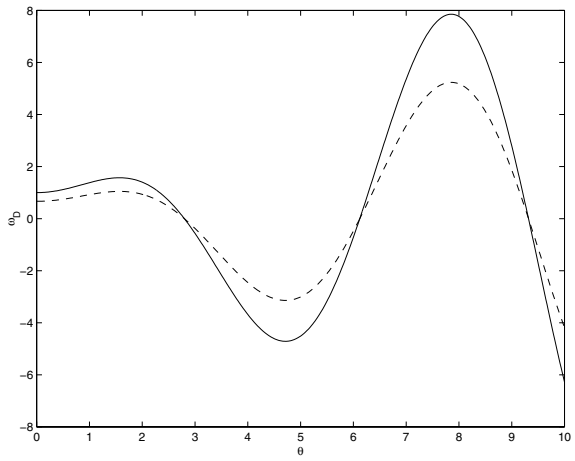

(a)

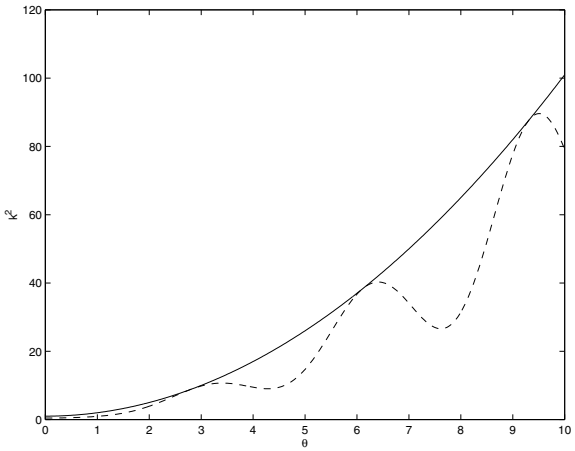

(b)

Figure 7. (a) The function $g(\theta)$ for $s = 1$ with $\kappa = 1$ (full curve) and $\kappa = 1.5$ (dashed curve); (b) the function $k(\theta)$ for $s = 1$ with $\kappa = 1$ (full curve) and $\kappa = 1.5$ (dashed curve).

to the lower ϵ_n stability threshold and destabilizing in the proximity of the upper threshold. The influence of κ through the FLR parameter is destabilizing in both cases.

The Shafranov shift has in general a very weak effect on the eigenfrequency both in the circular and the elongated cases. Figure 9 shows the growth rate as a function of the Shafranov shift with η_i as a parameter. The other parameters are $s = q = \tau = \epsilon_n = \kappa = 1$ with $\eta_i = 8$ (dashed dotted curve), $\eta_i = 6$ (dashed curve) and $\eta_i = 4$ (full curve). Similar results are obtained for small ϵ_n.

To quantify the effects of elongation and Shafranov shift on η_i-mode stability for realistic tokamak equilibria, parameters from the JET H-mode discharge 43633 have been studied. The stability calculation was performed at $\rho = 0.66$ in steady state at $t = 48$ s. The other parameters are $s = 0.45$, $q = 1.67$, $\tau = 1$, $\epsilon_n = 1.13$, $\kappa = 1.6$ and the Shafranov shift is -0.12. The stability calculation is most easily performed through a scaling in η_i values, this scaling is motivated by the large uncertainty in the experimental η_i values. For η_i values around

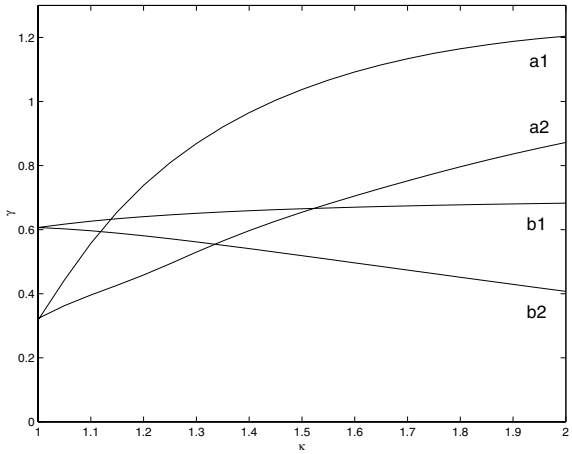

Figure 8. The growth rate (normalized to the electron diamagnetic drift frequency) versus κ for $q = s = \tau = 1$, $k_\perp^2 \rho^2 = 0.1$, $\eta_\mathrm{i} = 4$. Curves a1 ($\epsilon_n = 1$) and b2 ($\epsilon_n = 0.1$) are the full numerical simulations and a2 ($\epsilon_n = 1$) and b1 ($\epsilon_n = 0.1$) are the simulations with $\omega_\mathrm{D}(\theta, \kappa = 1)$.

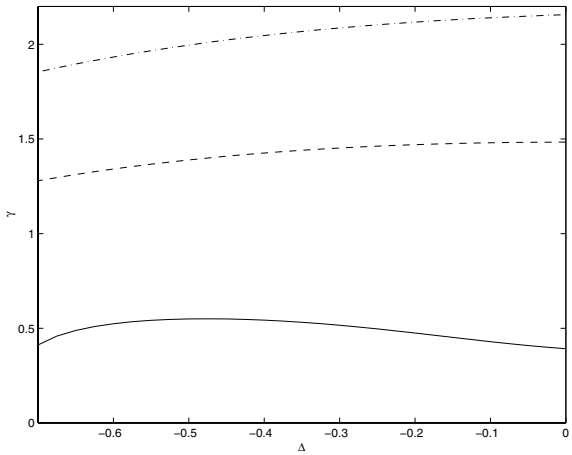

Figure 9. The growth rate (normalized to the electron diamagnetic drift frequency) versus Shafranov shift for $q = s = \tau = 1$, $k_\perp^2 \rho^2 = 0.1$, $\epsilon_n = 1$, $\kappa = 1$. $\eta_\mathrm{i} = 8$ (dashed dotted curve); $\eta_\mathrm{i} = 6$ (dashed curve) and $\eta_\mathrm{i} = 4$ (full curve).

4 the growth rate increases by approximately a factor of two when elongation is included. The Shafranov shift has a more modest contribution, a destabilizing effect of less than 20%. These results are rather typical for the JET equilibria considered.

4. Summary

The effects of plasma shaping on the stability of ion-temperature-gradient driven modes is investigated. The work is based on an advanced fluid model for the ions, which is extended to allow for non-circular cross sections. The electrons are assumed to be Boltzmann distributed. The derived eigenvalue equation (17), which includes effects of elongation κ and Shafranov shift, is solved numerically.

The main effect of elongation enters through a modification of the magnetic drift frequency ω_D. Also the FLR parameter and the parallel wavenumber $k_\parallel$ are modified. For large values of $\epsilon_n = \omega_D/\omega_\star$, corresponding to the flat density regime, it is found that the η_i-mode is slightly destabilized by elongation, whereas for small ϵ_n a stabilization is found. The influence of the Shafranov shift is found to be slightly stabilizing.

In addition, the spectrum of the unstable modes is shifted towards shorter wavelengths for elongated equilibria. This shift tends to reduce the transport by reducing the correlation length in the plasma. For realistic tokamak parameters, the model predicts a slight destabilization of the η_i-mode in the core plasma where the density profiles are rather flat. In the edge, on the other hand, a stabilizing effect is expected. To evaluate the total effect of elongation on the confinement time, both the edge region where κ is large, and the core region must be included in the analysis. To this end, a transport code simulation is needed which treats the core and edge transport processes self-consistently and which includes the effects of non-circular geometry on the resistive edge modes. This will be the subject of a future paper.

References

[1] Liewer P C 1985 *Nucl. Fusion* **25** 543
[2] Wagner F and Stroth U 1993 *Plasma Phys. Control. Fusion* **35** 1321
[3] Yshmanov P N *et al* 1990 *Nucl. Fusion* **30** 1999
[4] Hua D D, Yu Y Q and Fowler T K 1992 *Phys. Fluids* **34** 3216
[5] Weiland J Private communication
[6] Rudakov L I and Sagdeev R Z 1961 *Sov. Phys.–Dokl.* **6** 415
[7] Coppi B, Rosenbluth M N and Sagdeev R Z 1967 *Phys. Fluids* **10** 582
[8] Coppi B and Pegoraro F 1977 *Nucl. Fusion* **17** 969
[9] Guzdar P N, Chen L, Tang W M and Rutherford P H 1983 *Phys. Fluids* **26** 673
[10] Kesner J 1991 *Nucl. Fusion* **31** 511
[11] Waltz R E and Miller R L 1999 *Phys. Plasmas* **6** 4265
[12] Rewoldt G, Tang W M and Chance M S 1982 *Phys. Fluids* **25** 480
[13] Chu K R, Ott E and Manheimer W M 1978 *Phys. Fluids* **21** 664
[14] Bateman G, Kritz A H, Kinsey J E, Redd A J and Weiland J 1998 *Phys. Plasmas* **5** 1793
[15] Dimits A M *et al* 2000 *Phys. Plasmas* **7** 969
[16] Jarmèn A, Andersson P and Weiland J 1987 *Nucl. Fusion* **27** 941
[17] Nilsson J, Liljeström M and Weiland J 1990 *Phys. Fluids* B **2** 2568
[18] Guo S C and Weiland J 1997 *Nucl. Fusion* **37** 1095
[19] Weiland J 2000 *Collective Modes in Inhomogeneous Plasmas, Kinetic and Advanced Fluid Theory* (Bristol: IOP Publishing)
[20] Miller R L, Chu M S, Greene J M, Lin-Liu Y R and Waltz R E 1998 *Phys. Plasmas* **5** 973
[21] Connor J W, Hastie R J and Taylor J B 1979 *Proc. R. Soc.* A **365** 1